



1 **Ground mobile observation system for measuring**
2 **multisurface microwave emissivity**

3 Wenying He ^{1*,2} Hongbin Chen^{1,2} Yuejian Xuan¹ Jun Li¹ Minzheng Duan^{1,2}

4
5 1.Key Laboratory of Middle Atmosphere and Global Environment Observation, Institute of
6 Atmospheric Physics, Chinese Academy of Sciences, Beijing 100029, China

7 2.University of Chinese Academy of Sciences, Beijing 100049, China

8 **Abstract**

9 Large microwave surface emissivities with a highly heterogeneous distribution
10 make it challenging to use satellite microwave data to retrieve precipitation and to be
11 assimilated into numerical models over land. To better understand the microwave
12 emissivity over land surfaces, we designed and established a ground observation
13 system for the in situ observation of microwave emissivities over several typical
14 surfaces. The major components of the system include a dual-frequency polarized
15 ground microwave radiometer, a mobile observation platform, and auxiliary sensors
16 to measure the surface temperature and soil temperature and moisture; moreover,
17 observation fields are designed comprising five different land surfaces.

18 Based on the observed data from the mobile system, we preliminarily investigated
19 the variations in the surface microwave emissivity over different land surfaces. The
20 results show that the horizontally polarized emissivity is more sensitive to land
21 surfaces than is the vertically polarized emissivity: the former decreases to 0.75 over
22 cement and increases to 0.90 over sand and bare soil and up to 0.97 over grass. The
23 corresponding emissivity polarization difference is obvious over water (>0.3) and
24 cement (approximately 0.25) but reduces to 0.1 over sand and 0.05 over bare soil and
25 almost 0.01 or close to zero over grass; this trend is similar to that of the Tb



26 polarization difference. At different elevation angles, the horizontally/vertically
27 polarized emissivities over land surfaces obviously increase/slightly decrease with
28 increasing elevation angle but exhibit the opposite trend over water.

29 Key words: Ground mobile observation system, microwave radiometer, microwave surface
30 emissivity, surface temperature, land surface

31

32 **1 Introduction**

33 The land surface microwave emissivity varies but is generally high (~ 0.90) and
34 thus generates strong surface radiance; however, this strong surface radiance obscures
35 the atmospheric radiance, making it more difficult to assimilate and precisely retrieve
36 atmospheric parameters using satellite microwave data over land (McNally et al.,
37 2000; Farbou et al., 2005; Schwartz et al., 2012). Moreover, due to complex variations
38 affected by many surface factors, such as soil type, wetness, vegetation type and
39 surface roughness, the land surface emissivity is poorly understood. Hence, the land
40 surface microwave emissivity constitutes a major parameter limiting the application
41 of spaceborne microwave data over land.

42 Microwave emissivity models have been developed only for a limited range of
43 frequencies and surface conditions. For example, the emissivity over bare soil was
44 modeled at lower frequencies, and the soil dielectric constants were obtained from
45 ground-based measurements (Wang and Schmugge, 1980). Furthermore, the
46 emissivity over the vegetation canopy was simulated using a radiative transfer model
47 with a large number of canopy optical parameters (Mo and Schmugge, 1987; Isaacs et
48 al., 1989; Fung, 1994). Weng (2001) developed a microwave land emissivity model to



49 quantify the emissivity over various surface conditions, including snow, deserts, and
50 vegetation. Xie et al. (2017) developed a parameterized soil surface emissivity model
51 for bare soil surfaces and compared with Weng's model, results reflected the reduced
52 overall errors, especially for horizontal polarization. Ultimately, the microwave
53 emissivity of land surfaces is determined mainly by the soil dielectric constant, which
54 is influenced by the physical temperature, soil texture and moisture content, and
55 vegetation structure and type. As a result of these complicated parameters with
56 numerous uncertainties, establishing a common physical emissivity model and
57 accurately obtaining emissivity estimates by using only an emissivity model remain
58 challenging.

59 Satellite observations offering extensive coverage have been used to estimate the
60 regional and global distributions of land surface emissivity since the 1990s (Prigent et
61 al., 2000; Moncet et al., 2011). To avoid the impacts of the complex variability of
62 clouds and precipitation in the atmosphere, only the brightness temperatures observed
63 by spaceborne microwave instruments under clear sky conditions are generally
64 selected to calculate the land surface microwave emissivity. Jones and Vonder Haar
65 (1997) used SSM/I (Special Sensor Microwave Imager) microwave observations and
66 GOES/VISSR (Geostationary Operational Environmental Satellite/Visible Infrared
67 Spin-Scan Radiometer) infrared data that were closely matched in both space and time
68 to retrieve the microwave land emissivity over the Central United States and utilized
69 the infrared data with a constant infrared emissivity of 0.98 to calculate the land skin
70 temperature (LST) under clear sky conditions. Further, Ruston and Vonder Haar (2004)



71 directly employed spatially varying infrared surface emissivities in the retrieval of
72 LST to calculate the microwave emissivity and discovered that the
73 atmospheric-corrected microwave surface emissivity is valuable for determining land
74 surface characteristics but is sensitive to rain events. Prigent et al. (1997, 1999)
75 calculated the land surface microwave emissivity over Africa, some parts of Europe
76 and West Asia by combining SSM/I data with LST observations provided by ISCCP
77 (International Satellite Cloud Climatology Project). With subsequently improved
78 ISCCP LST and cloud product data, Prigent et al. (2006) presented a global land
79 surface microwave emissivity database retrieved from 10 years of SSM/I data and
80 plotted the monthly average land surface microwave emissivity onto a geographic
81 map. In their work, the microwave emissivity retrieval was based primarily on
82 radiative transfer calculations, in which infrared data were used to determine the LST
83 under clear sky conditions, and atmospheric sounding data were used to take the
84 effects of atmospheric attenuation into account. Nevertheless, due to the complexity
85 and variability of clouds and atmospheric precipitation, land surface microwave
86 emissivity estimates derived from satellite observations are available only under clear
87 sky conditions. Moreover, the cloud screening and LST retrieval methods still contain
88 numerous uncertainties, which represent the main sources of errors in emissivity
89 calculations.

90 At present, the accuracy of surface emissivity estimates calculated from either
91 emissivity models or satellite observations is limited by the complexity of the land
92 surface and the variability of vegetation types and soil moisture. Hence, surface



93 emissivity calculations need to be verified and improved with more in situ observation
94 data.

95 To better understand the variation characteristics of surface emissivity with
96 surface conditions, Ulaby et al. (1985) combined field experiments and theoretical
97 research and revealed that the land surface microwave specific emissivity is strongly
98 correlated with the distributions of soil moisture and vegetation. In addition, a few
99 observation experiments using ground-based microwave radiometers have been
100 carried out since the 1990s to study the variation characteristics of emissivity over
101 different surfaces (Njoku and O'Neill, 1982; Matzler, 1990, 1994; Calvet, 1997;
102 Wigneron, 1994; Morland et al., 1995). More recently, in situ passive microwave
103 radiometer measurements over snow cover and sub-Arctic frozen soil have been used
104 to validate empirical emission models (Lemmetyinen et al., 2015; Montpetit et al.,
105 2018). Additionally, an aircraft-flown microwave radiometer was used to directly
106 observe the surface emissivity over forests, crops, snow and ice to analyze the
107 sensitivity of those emissivities to the view angle, frequency, measurement time and
108 surface characteristics (Hewison, 2001; Wigneron et al., 1997; Hewison and English,
109 1999).

110 The observation mode of a microwave radiometer in a field experiment is an
111 important consideration. Usually, ground-based radiometers are fixed when scanning
112 the observed field; for example, they can be mounted on a truck or a tower (Matzler,
113 1990; Lemmetyinen et al., 2015), allowing the instrument to better determine the
114 temporal evolution of surface emissivity over single type of land-cover area. In



115 contrast, using a mobile mode, such as airborne and mobile sled-based radiometers
116 (Morland, 2003; Lemmetyinen et al., 2015; Montpetit et al., 2018), can better reveal
117 the spatial evolution of surface emissivity over different land-cover areas, but it is not
118 easy to obtain long-term emissivity observations due to the high cost and effort.

119 To obtain the long-term temporal evolution of surface emissivity over different
120 types of surfaces simultaneously, we proposed and developed a ground mobile
121 observation system to enhance in situ microwave emissivity observations. Long-term
122 continuous emissivity field experiments can help to more accurately understand the
123 characteristics of passive microwave polarized emissivities over typical land surfaces,
124 form a benchmark for verifying the retrieved emissivities from satellite or emission
125 models, and establish an emissivity parameterization scheme for a given surface in
126 radiance assimilation. The outline of this paper is as follows: the design of the ground
127 mobile observation system for measuring surface emissivity is introduced in section 2;
128 the data and method used for the emissivity calculations are described in section 3;
129 then, the surface emissivity estimates obtained directly from the observation system
130 are discussed preliminarily in section 4; and a final short summary is given in section
131 5.

132 **2. Ground mobile observation system for surface microwave emissivity**

133 To obtain the surface emissivity over several typical surfaces simultaneously, we
134 designed a ground mobile observation system to carry out long-term field experiments
135 over 5 test plots. Fig. 1 is an on-site photo of the observation system operating at the
136 Xianghe observation site (116.98° E, 39.76° N), Hebei Province, China. As shown in



137 Fig. 1, the mobile observation system consists of five main parts: a dual-polarized
138 ground-based microwave radiometer to observe the surface and sky radiances, a
139 mobile platform to move back and forth along a track, and three auxiliary sensors to
140 measure the surface temperature, soil temperature and moisture. The observation field
141 includes five test plots, namely, water, cement, sand, bare soil and grass. From the
142 observation system, we can directly obtain surface microwave emissivity estimates
143 more accurately than is possible from satellite data or emissivity models, which is
144 important to properly understand the variation characteristics of land microwave
145 emissivities and to improve the emissivity parameterization schemes used in models.



146
147 Fig 1 On-site photo of the surface microwave emissivity observation system
148 operating over various surfaces at the Xianghe site, China
149

150 2.1 Ground-based microwave radiometer

151 The core device of the observation system is a dual-frequency (18.7 and 36.5
152 GHz), dual-polarized (horizontal and vertical) microwave radiometer (RPG-4CH-DP)
153 produced by Radiometer Physics GmbH, Germany. The RPG-4CH-DP radiometer is a



154 high-performance instrument with a direct detection receiver and a completely
155 automatic calibration system. The radiometer is mounted on an accurate
156 elevation/azimuth positioner so that the whole system can perform scans in any
157 direction from the sky to the ground, thereby realizing complex scanning schemes,
158 such as all-sky monitoring and all-round monitoring of the ground. The RPG-4CH-DP
159 can distinguish cloud/raindrop particles during precipitation and monitor soil moisture
160 and vegetation parameters by using signals with different polarizations. Both
161 frequencies of 18.7 GHz and 36.5 GHz have been widely combined to detect snow
162 depth and snow water content and are frequently used in most spaceborne microwave
163 imagers, such as the SSM/I, AMSR-E (Advanced Microwave Scanning Radiometer
164 for EOS) and GMI (Greenhouse gases Monitoring Instrument) sensors. The directly
165 observed surface emissivities at these two frequencies can provide highly accurate
166 references for the verification and assimilation of spaceborne microwave
167 observations.

168 The RPG-4CH-DP radiometer has a comparable half-power beam width of
169 approximately 6° and a calibration accuracy of ± 1 K. Currently, the height of the
170 instrument above the ground is 2.5 m, which results in a half-power footprint width of
171 0.22 m on average. More details regarding the instrument specifications for the
172 RPG-4CH-DP are shown in Table 1.

173
174

Table 1 Instrument Specifications

Parameter	Specification
Radiometric resolution	0.2 K RMS (1.0 s integration time)
Optical resolution	HPBW: 6.0° (Sidelobe level < -30 dBc)



Absolute system stability	1.0 K
Receiver and antenna thermal stabilization	Accuracy <0.05 K
Pointing speed	Elevation: 3°/sec, azimuth: 5°/sec
Radiometric range	0-350 K
Operating temperature range	-40°C to +45°C
Power consumption	<350 watts on average, 500-watt peak
Weight	105 kg for receiver modules, 300 kg for positioner

175

176 Currently, the RPG-4CH-DP provides only the basic brightness temperature (T_b)
177 data in 4 channels without other related products. By incorporating the auxiliary
178 observations from the observation system, we broadened the application of the
179 instrument, denoted RPG-XCH-DP, thereby providing not only the basic microwave
180 radiance but also the complex surface emissivity.

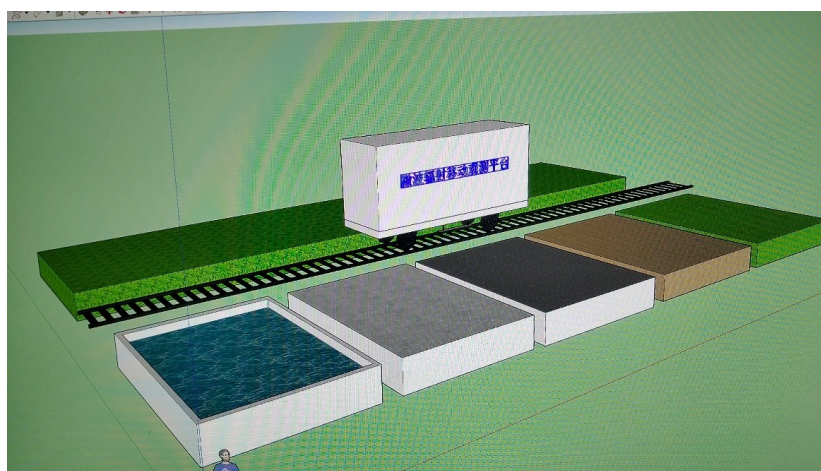
181 **2.2 Mobile system (platform)**

182 The multitarget mobile system comprises a track, a mobile platform, a driving
183 system and a control unit. As the sketch of the mobile system in Fig. 2 shows, the 25
184 m track is parallel to the test plots with an observation interval of 0.3 m. The mobile
185 platform placed on the track is a metal box 4 m in length, 0.8 m in height, and 1.0 m
186 in depth. The driving system includes a stepper motor, transmission mechanism, and
187 communication cable connected to the mobile platform and power supply. The control
188 unit consists of a single-chip microcomputer, timer and stepper motor driver, which
189 can set the moving time and control the operation of the driving device. The control
190 device is installed on the mobile platform and connects both driving devices.

191 In this experiment, to obtain the microwave emissivity over different surfaces in
192 near-simultaneous time, the RPG-4CH-DP is mounted on the mobile platform and
193 moves back and forth along the track. The communication system for receiving the
194 data and the power supply are placed in the metal box. According to the commands
195 from the single-chip microcomputer and the driving force from the stepper motor, the
196 mobile platform moves along the track similar to a small train, and the onboard



197 radiometer scans the 5 test plots at fixed times every day.



198

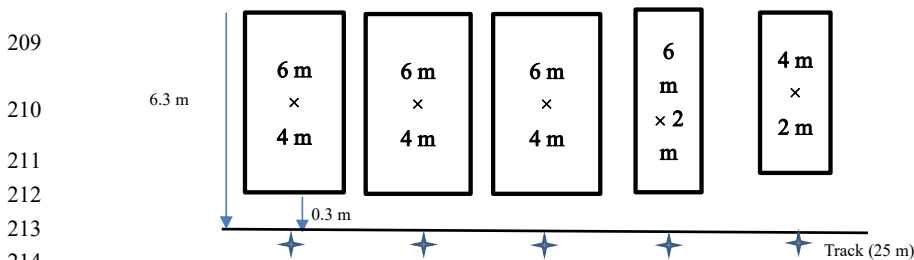
199

Fig. 2 Sketch of the mobile platform

200 2.3 Observation field and auxiliary data

201 Fig. 3 shows a sketch of the observation field, including the 5 test plots
 202 distributed along the 25 m track. Currently, 5 surface types are considered in the
 203 observation field, namely, water, cement, sand, soil and grass. For the water body, a
 204 plastic pool 6 m long and 2.4 m wide is used to hold the water. The adjacent cement
 205 surface consists of a 2 m wide footpath. The remaining three plots of sand, bare soil
 206 and grass are the same size (approximately 6 m long by 4 m wide) and are separated
 207 by a distance of approximately 2 m.

208



209

210

211

212

213

214

215 Fig. 3 Sketch of the observation field (including 5 test plots: water, cement, sand,
 216 bare soil and grass), where \star denotes the position of a touching switch

217

218 To scan each plot at the same place at a fixed time, five touching switches



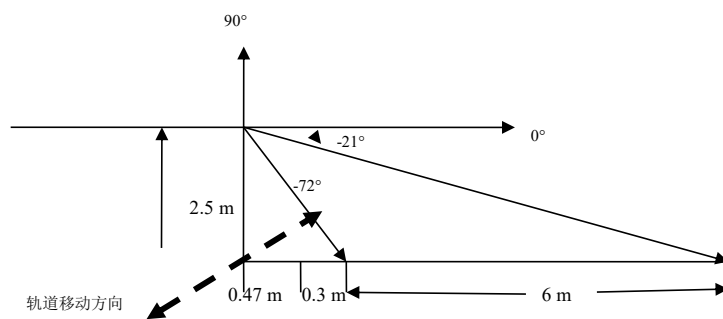
219 corresponding to the center of each plot are fixed on the track to stop the moving
220 platform so that the radiometer can scan the same place for a couple of minutes. By
221 using this mobile platform, the ground-based radiometer can scan multiple surfaces
222 almost simultaneously (i.e., within 1 hr), thereby providing valuable measurements
223 for understanding the variation in surface emissivity over different land surfaces with
224 different characteristics.

225 The auxiliary data include mainly the surface temperature, soil temperature and
226 soil moisture. Five thermometers with a PT100 temperature sensor made by
227 Honeywell company are placed separately on each test plot to measure their surface
228 temperature. In addition, an SI-111 precision infrared radiometer developed by
229 Apogee Instruments Inc. is fixed on a stand of the RPG-4CH-DP radiometer to obtain
230 the surface temperature of each plot while the microwave radiometer is moving.
231 Furthermore, a set of soil temperature and humidity sensors is fixed at three soil
232 depths, 5 cm, 10 cm and 20 cm, to detect the subsurface soil temperature and humidity.
233 To monitor the real-time working situation of the whole observation system, a digital
234 video camera is installed near the field to record the states of the mobile platform and
235 radiometer as well as changes in the weather, such as the presence of cloud cover, rain
236 or snow.

237 **2.4 Scanning mode**

238 To directly obtain the surface emissivity, a combined mode of ground
239 observations at multiple elevation angles and zenith observations is designed, in
240 which the former monitors mainly the surface radiance while the latter monitors the
241 sky radiance in the same 1 hr period.

242 The ground observation mode is illustrated in Fig. 4. The mobile platform is
243 triggered every hour, and the microwave radiometer operates using the ground
244 scanning mode at this time. The scan is performed from the horizon (0°) to the ground,
245 and the elevation angle is defined as the angle between the scanning direction and the
246 horizontal. A negative value indicates an angle below the horizon, which is equivalent
247 to $90^\circ - \theta$, where θ is the incident angle, an important parameter for describing
248 spaceborne radiometer scanning. The radiometer is 2.5 m above the ground, so it can



249

250 Fig. 4 Sketch of the combined scanning mode of the microwave radiometer

251

252 scan each test plot with a length of 6 m when the elevation angle is between -21° and
253 -72° , as shown in Fig. 4. The valid elevation angle range for water is different due to
254 the different length of the pool. To determine the surface emissivity variation with the
255 elevation angle, the radiometer is set to scan each test plot with an angle interval of 3°
256 from -21° to -45° , an angle interval of 5° from -45° to -70° , and then back to -21° to
257 scan the test plot repeatedly during the ground observation mode. To acquire ground
258 observations over all 5 test plots within 1 hr, each plot is given 9 minutes; in other
259 words, the mobile platform will move to the cement plot at 9 min, the sand plot at 18
260 min, the bare soil plot at 27 min, and finally the grass plot at 36 min. After finishing
261 the ground observations in all 5 test plots, the mobile platform will begin to move
262 back at 45 min and reach the beginning location after approximately 6 min. During
263 the return trip, the scan mode changes to the zenith observation mode so that the
264 radiometer scans from the ground to the sky. When the elevation angle is raised to 90° ,
265 the radiometer will continually acquire zenith observations for approximately 5 min to
266 obtain the sky radiance. After obtaining these zenith observations, the elevation angle
267 changes from the zenith observation mode to the ground observation mode at -21° so
268 that the radiometer is already in the ground observation mode when the next
269 measurement cycle arrives. In this way, the radiometer on the mobile platform can
270 obtain not only the ground radiance over 5 test plots but also the sky radiance within a
271 1 hr period. Here, we assume that 1 hr is short enough to neglect the minute-scale



272 differences in the surface and sky radiance, and thus, the mobile system can obtain the
273 microwave emissivity over different surfaces nearly simultaneously.

274

275 **3 Data and method**

276 Three types of observation data are obtained from the field experiment: the
277 microwave brightness temperature (T_b) at different scanning angles from the ground
278 microwave radiometer; the surface temperature (T_s) of the five test plots measured
279 from the ground thermometers and infrared sensor; and the soil temperature and
280 moisture at three depths in the sand and bare soil plots.

281 When ground microwave radiometer scans the surface, the measured T_b comes
282 mainly from two contributions: that of upward radiation from the surface and that of
283 the reflected downward atmospheric radiance. Thus, the measured T_b can be
284 approximately expressed by Eq. (1):

$$285 \quad T_b = \varepsilon T_s + (1 - \varepsilon) T_{sky} \quad (1)$$

286 where ε is the surface emissivity, T_s is the surface temperature, and T_{sky} is the radiance
287 from the sky. From Eq. (1), the surface emissivity can be directly calculated using Eq.
288 (2) by combining the T_b contributions from the surface and sky with the surface
289 temperature synchronously measured from the infrared sensor in the observation
290 system.

$$291 \quad \varepsilon = (T_b - T_{sky}) / (T_s - T_{sky}) \quad (2)$$

292 Through applying the ground mobile observation system for surface microwave emissivity and
293 combining the video camera records with the soil temperature and moisture measurements, we can
294 not only directly obtain highly accurate surface microwave emissivity observations over different
295 test plots but also investigate the variation characteristics of the surface emissivity under different
296 weather conditions.

297

298 **4. Preliminary results**

299 Considering both the viewing field of the microwave radiometer and the size of the



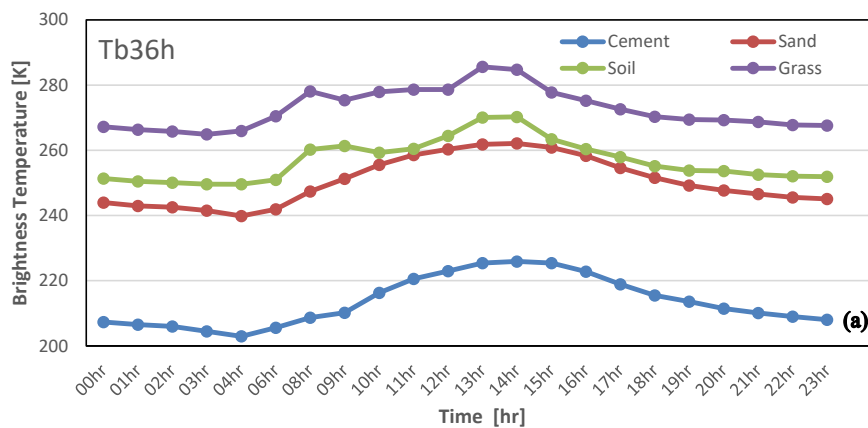
300 test plots, the elevation angle range between -24° and -65° is chosen for observing the
301 land test plots (cement, sand, soil and grass), while elevation angles between -33° and
302 -65° are valid for observing the water surface. Here, we focus on the variations in the
303 radiance and surface emissivity over the 5 test plots during the observations recorded
304 in October 2018 under clear sky conditions.

305 **4.1 Radiance**

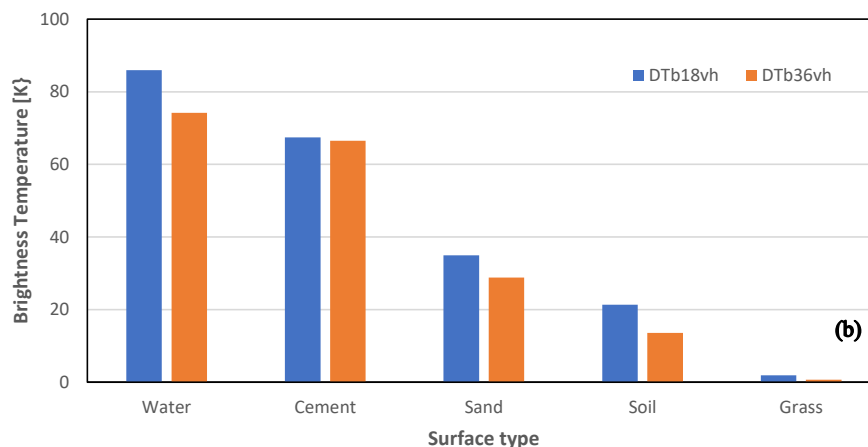
306 Since a scanning angle of 36° is equivalent to an incident angle of 54° used for
307 many spaceborne microwave imagers, such as AMSR-E (55°) or SSM/I (53°), we first
308 compare the variation in the observed Tb over different surfaces at an elevation angle
309 of 36° . The changes in the observed Tb at 36.5 GHz in horizontal (Tb36h) and vertical
310 (Tb36v) polarization over the four land surfaces within 24 hr (Beijing Time, BJT) are
311 quite similar, with smaller values at night and larger values at noon. Less variation in
312 the radiance is noted at Tb36v (not shown), but more significant variations are
313 detected at Tb36h over the four surfaces as shown in Fig. 5a: the observed Tb36h
314 from grass is approximately 270-285 K but varies within 240-270 K over sand and
315 bare soil and reaches only 200-230 K for cement. The observed Tb at 18.75 GHz
316 within 24 h shows similar variations with only slight changes among the different
317 land surfaces. Likewise, the corresponding polarization differences (V-H) of Tb
318 within 24 hr are very similar to one another, so both DTb18vh and DTb36vh at 02:00
319 (BJT) are shown in Fig. 5b, revealing a slight difference (close to zero) for grass but
320 considerably larger differences for water and cement (almost up to 70 K for water)
321 and smaller differences over sand and soil (below 30 K). In addition, the values of



322 DTb18vh are larger than those of DTb36vh. The Tb polarization difference is more
 323 significant over water than over land and is closely related to the roughness of the
 324 land surface. In addition, the roughness of grass is obviously larger than that of the
 325 other three land surfaces and thus scatters more surface radiance and reduces the
 326 polarization difference. Therefore, the observed Tb polarization differences over the
 327 different surfaces shown in Fig. 5b appear reasonable, and the given quantitative
 328 polarization differences for certain surfaces can serve as a valid reference for
 329 identifying land surfaces and water bodies.



330



331

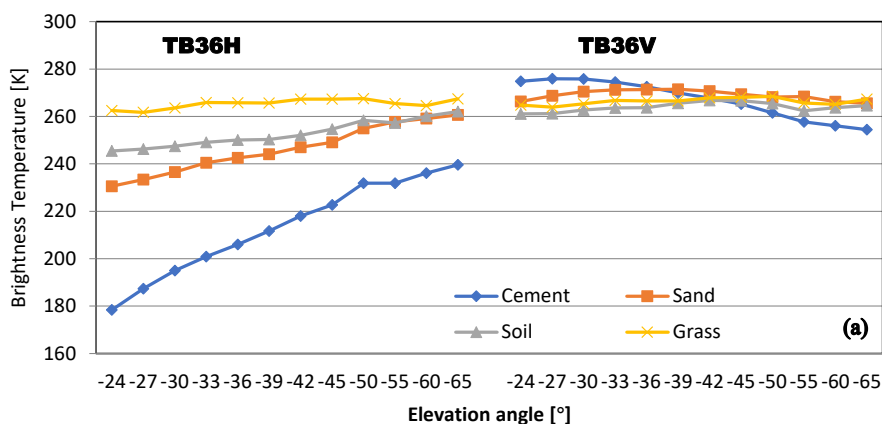


332 Fig. 5 Variations in the observed Tb (a) and Tb polarization differences (b) over
333 different surfaces in October 2018.

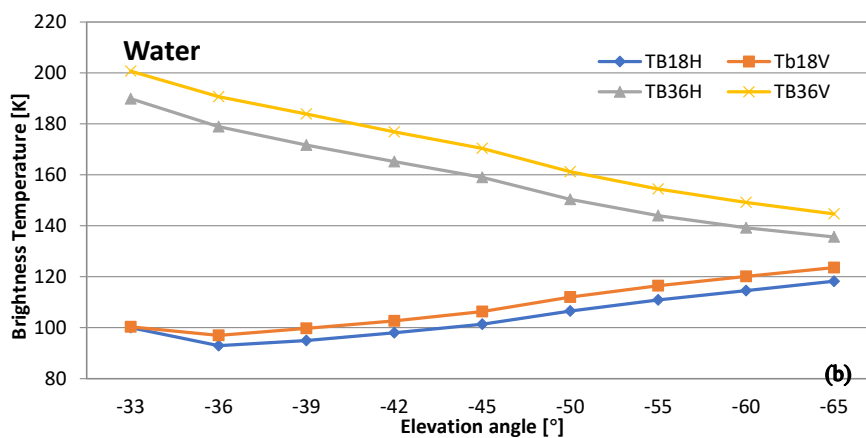
334 To study the variations in Tb at more than a single angle, Fig. 6a shows the changes in
335 the observed Tb with the elevation angle ranging from 24° to 65° over the four land
336 surfaces. The horizontally polarized Tb is clearly more sensitive to land surfaces than
337 the vertically polarized Tb with increasing elevation angle; in particular, Tb_{36h} rises
338 rapidly from 180 K to 240 K over cement but slowly increases from 240 K to 260 K
339 over sand and bare soil and remains almost constant over grass. In contrast, the
340 variations in the vertically polarized Tb with increasing elevation angle are similar
341 among the land surfaces and are smaller than those in the horizontally polarized Tb,
342 showing a decreasing trend from 280 K to 260 K over different surfaces. In addition,
343 the variations in the observed Tb over water are presented in Fig. 6b. Different from
344 the above observations over land surfaces, the vertically polarized Tb over water
345 obviously reduces from 200 K to 140 K with increasing elevation angle, while the
346 horizontally polarized Tb slowly rises from 100 K to 120 K, almost opposite to the Tb
347 polarization variations over land surfaces. The corresponding changes in the
348 polarization difference of Tb at 18.75 GHz (DTb_{18vh}) over all 5 classes of surfaces
349 are further plotted in Fig. 6c. In general, the Tb polarization difference decreases with
350 increasing elevation angle, and the varied ranges with the elevation angle over the 5
351 classes surfaces in Fig. 6c are similar to those in Fig.5b; thus, the decreasing trend is
352 most obvious over water and cement and least evident over grass with increasing
353 elevation angle. Furthermore, the variations of the Tb polarization difference at 36.5



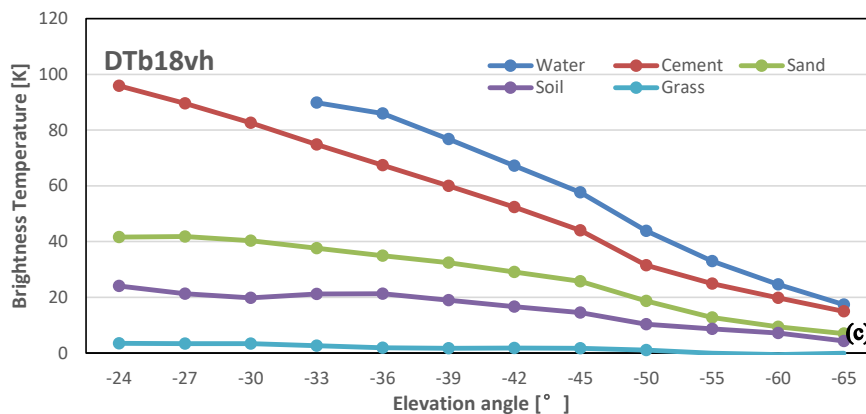
354 GHz with the elevation angle are similar to those at 18.75 GHz over all 5 test plots.



355



356



357

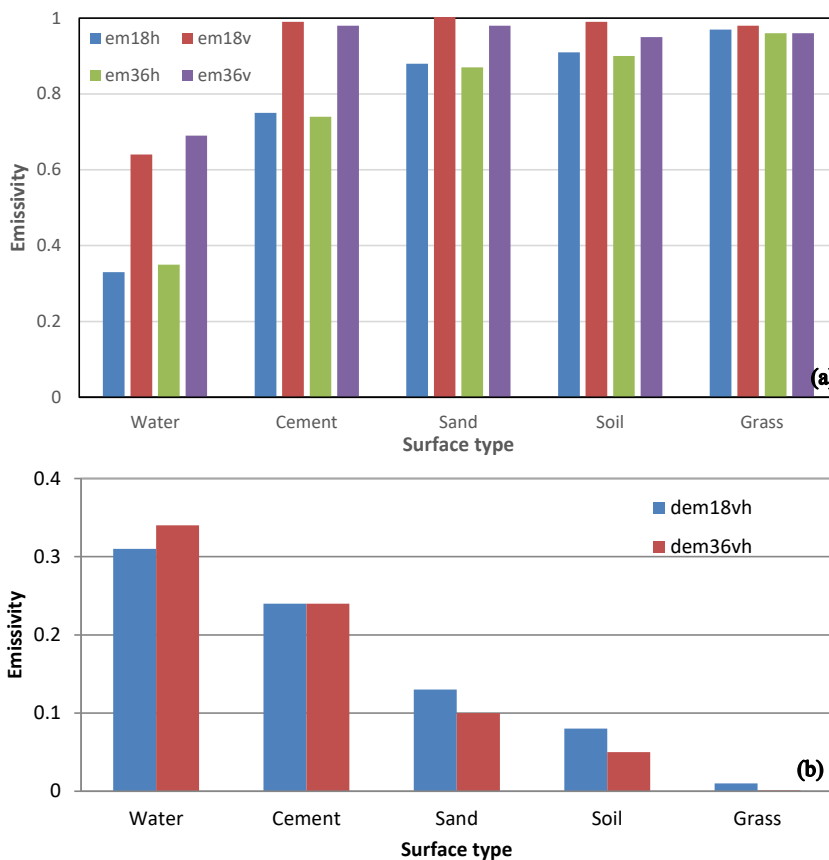
358 Fig. 6 Variations in the observed radiance over different land surfaces with the



359 elevation angle

360 **4.2 Surface microwave emissivity**

361 Combining the surface and sky radiance contributions to T_b with the surface
362 temperature derived from the infrared sensor, the surface emissivity (ϵ) is derived
363 from Eq. (2). Since the diurnal variation of ϵ is more constant and less significant than
364 that of the T_b radiance, the surface emissivity observed at 02:00 (BJT) is chosen for
365 the following investigation. First, the polarized ϵ at both 18.75 and 36.5 GHz and their
366 polarization differences at an elevation angle of 36° are compared in Fig. 7a. The
367 vertically polarized ϵ (ϵ_v) is clearly much larger than the horizontally polarized ϵ (ϵ_h),
368 and the ϵ values at the same frequencies are close, but the ϵ values over water is
369 smaller than those over the four land surfaces. The ϵ_h values obviously differ among
370 the 4 land surfaces, although their corresponding ϵ_v values are relatively similar,
371 exceeding 0.95, which indicates that ϵ_h is more sensitive to land surfaces than ϵ_v . The
372 ϵ_h is lower than 0.75 over cement but increases to 0.90 over sand and bare soil and up
373 to 0.97 over grass. Thus, the polarization difference ($\epsilon_v - \epsilon_h$) shown in Fig. 7b is
374 obvious over water (>0.3) and cement (approximately 0.25) but reduces to 0.1 over
375 sand and 0.05 over bare soil and almost 0.01 or close to zero over grass; this trend is
376 similar to that of the T_b polarization difference shown in Fig. 5b.



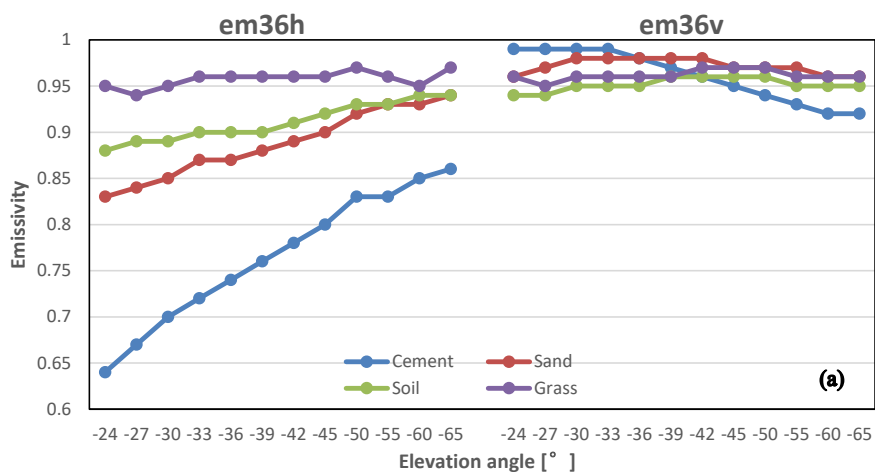
377

378

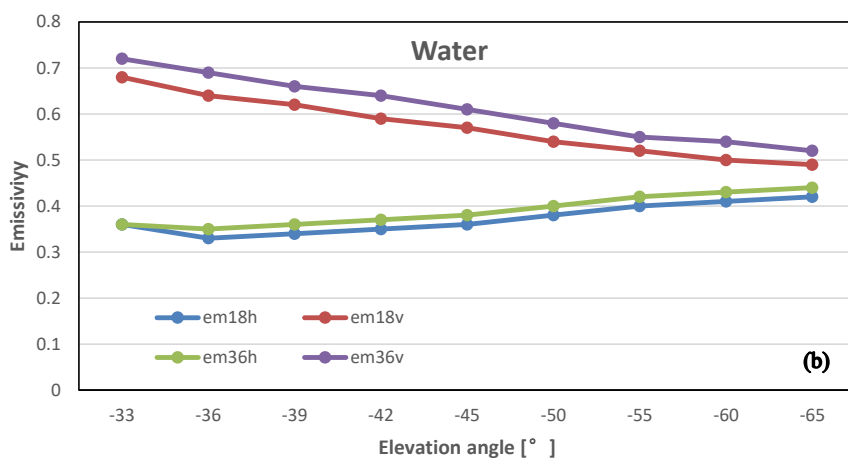
379 Fig. 7 Variations in the surface emissivity over different land surfaces at the

380 elevation angle of 36°

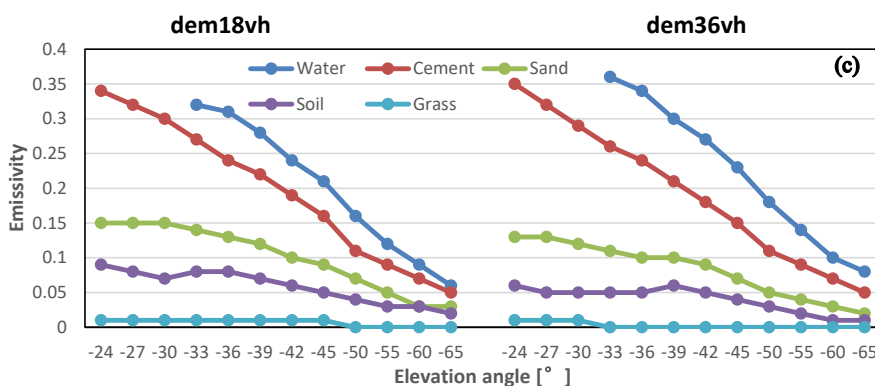
381 In addition to investigating the variations at a fixed angle, the variations in ϵ at
382 multiple elevation angles over the 4 land surfaces are compared in Fig. 8a. Because ϵ_h
383 is more sensitive to land surfaces than to water, when the elevation angle changes
384 from -24° to 65°, ϵ_h clearly rises from 0.65 to 0.85 over cement, followed by sand and
385 bare soil with ϵ_h increasing from 0.85 to 0.95, and ϵ_h is constant at 0.95 over grass.
386 The corresponding ϵ_v values over the four land surfaces are closer and exhibit a
387 slightly decreasing trend within the range of 0.9-1.0 with increasing elevation angle.



388



389



390

391 Fig. 8 Variations in the surface emissivity over different land surfaces(a,b) and

392 their ϵ polarization differences(c) with increasing elevation angle.



393 As shown in Fig. 8b, the ϵ values over water show considerably different variation
394 trends with the elevation angle from those over land surfaces: when the elevation
395 angle changes from -33° to -65° , ϵ_v reduces from 0.7 to 0.5, while ϵ_h slightly increases
396 within the vicinity of 0.4. The ϵ polarization differences ($\epsilon_v - \epsilon_h$) in Fig. 8c present
397 similar variation trends to those shown in Fig. 7b; that is, the ϵ polarization difference
398 decreases with increasing elevation angle, and the larger the polarization difference of
399 ϵ is (Fig. 7b), the greater the variation with the elevation angle (Fig. 8c). Hence, the
400 decreasing trend of ϵ is most obvious over water and cement, and ϵ slightly changes
401 over grass with increasing elevation angle. The variation in the ϵ polarization
402 difference at 36.5 GHz with the elevation angle is similar to that at 18.75 GHz over all
403 5 test plots (results not shown).

404

405 **5 Summary**

406 In this paper, we introduce a ground mobile observation system for directly
407 obtaining surface microwave emissivity estimates over five types of surfaces: water,
408 cement, sand, soil and grass. The mobile observation system consists mainly of a
409 dual-polarized ground-based microwave radiometer, a mobile platform, and auxiliary
410 sensors, and the observation field comprises 5 test plots.

411 Based on the observed data from the mobile system, we preliminarily
412 investigated the variation characteristics of the surface microwave emissivity over the
413 five different land surfaces. The results show that the horizontally polarized
414 emissivity is more sensitive to land surfaces than is the vertically polarized emissivity:



415 the former decreases to 0.75 over cement and increases to 0.90 over sand and bare soil
416 and up to 0.97 over grass. Hence, the corresponding polarization difference is obvious
417 over water (>0.3) and cement (approximately 0.25) but reduces to 0.1 over sand and
418 0.05 over bare soil and almost 0.01 or close to zero over grass; this trend is similar to
419 that of the T_b polarization difference. For different elevation angles, the
420 horizontally/vertically polarized emissivities over the land surfaces obviously
421 increase/slightly decrease with increasing elevation angle but exhibit the opposite
422 trend over water. Moreover, the emissivity polarization difference decreases with
423 increasing elevation angle, and the larger the emissivity polarization difference is over
424 a certain surface, the greater the variation with the elevation angle.

425 We developed a ground mobile observation system for measuring the microwave
426 emissivity over multiple surfaces, and the system has worked stably since August
427 2018. The preliminary results from our observation system partly reflect similar
428 variation trends to those reported by previous surface emissivity experiments, and
429 some are more related to the variation in emissivity at different elevation angles. In
430 future research, we will carry out further analyses and refine the emissivity
431 parameterization scheme for given surfaces based on long-term observations.

432

433 **Acknowledgments**

434 This work was supported by National Natural Science Foundation of China [No.
435 41575033] and National Key Research and Development Program of China
436 [2017YFC1501700]. We thank the staff at the Xianghe site for their maintenance
437 work on the microwave radiometer and the ground mobile observation system.

438

439 **References**



- 440 Calvet, J. C., Wigneron J. P., Chanzy. A., Raju S., and Laguerre L.: Microwave dielectric
441 properties of a silt-loam at high frequencies, *IEEE Trans. Geosci. Remote sensing*, 33,
442 634-642, doi: 10.1109/36.387579, 1995.
- 443 Fung A. K.: *Microwave Scattering and Emission Models and Their Applications*. Norwood, MA:
444 Artech House, 1994.
- 445 Karbou, F., Aires F., Prigent C., and Eymard L.: Potential of Advanced Microwave Sounding
446 Unit-A (AMSU-A) and AMSU-B measurements for atmospheric temperature and humidity
447 profiling over land, *Journal of Geophysical Research*, 110, D07109,
448 doi:10.1029/2004JD005318, 2005.
- 449 Hewison T. J.: Airborne measurements of forest and agricultural land surface emissivity at
450 millimeter wavelengths. *IEEE Trans. Geosci. Remote sensing.*, 39, 393-400,
451 DOI:10.1109/36.905247, 2001.
- 452 Hewison, T. J., and English S. J.: Airborne retrievals of snow and ice surface emissivity at
453 millimeter wavelengths. *IEEE Trans. Geosci. Remote Sens.*, 37, 1871-1887,
454 doi:10.1109/36.774700, 1999.
- 455 Isaacs R. G., Jin Y. Q., Worsham R. D., Deblonde, G., Falcone, V. J.: The RADTRAN microwave
456 surface emission models. *IEEE Trans. Geosci. Remote sensing*, 27, 433-440,
457 DOI:10.1109/36.29563, 1989.
- 458 Jones, A.S., Vonder Haar, T.H.: Retrieval of microwave surface emittance over land using
459 coincident microwave and infrared satellite measurements, *J. Geophys. Res.*, 102, 13,609-13,626,
460 <https://doi.org/10.1029/97JD00797>, 1997.
- 461 Lemmetyinen, J., Derksen C., Toose, P., Proksch, C., Pulliainen, J., Kontu, A., Rautiainen, K.,
462 Seppänen, J., Hallikainen, M.: Simulating seasonally and spatially varying snow cover
463 brightness temperature using HUT snow emission model and retrieval of a microwave effective
464 grain size, *Remote Sens. Environ.*, 156, 71-95, <http://dx.doi.org/10.1016/j.rse.2014.09.016>, 2015
- 465 Mazler C.: Seasonal evolution of microwave radiation from an oat field, *Remote Sens. Environ.*,
466 31, 161-173, doi:10.1016/0034-4257(90)90086-2, 1990.
- 467 Mazler C.: Passive microwave signatures of landscapes in winter, *Meteorol. Atmos. Phys.*, 54,
468 241-260, <https://doi.org/10.1007/BF01030063>, 1994.
- 469 McNally A. P., Derber J. C., Wu W. S., Katz, B.B.: The use of TOVS level-1B radiances in the
470 NCEP SSI analysis system, *Quarterly Journal of the Royal Meteorological Society*, 126,
471 689-724, <https://doi.org/10.1002/qj.49712656315>, 2000.
- 472 Mo, T., Schmugge, T.J.: A parameterization of the effect of surface roughness on microwave
473 emission, *IEEE Trans. Geosci. Remote Sens.*, 4, 481-486, doi: 10.1109/TGRS.1987.289860,
474 1987.
- 475 Moncet, J.L., P. Liang, J. F., Galantowicz, et al., 2011: Land surface microwave emissivities
476 derived from AMSR-E and MODIS measurements with advanced quality control. *J. Geophys.*
477 *Res.*, 116, D16104, doi:10.1029/2010JD015429.
- 478 Montpetit, B., Royer, A., Roy, A., Langlois, A.: In-situ passive microwave emission model
479 parameterization of sub-arctic frozen organic soils, *Remote Sens. Environ.*, 205, 112-118,
480 <http://dx.doi.org/10.1016/j.rse.2014.09.016>, <https://doi.org/10.1016/j.rse.2017.10.033>, 2018.
- 481 Morland, J. C., Grimes D.I.F., Dugdale, G., Hewison, T.J.: The Estimation of Land Surface
482 Emissivities at 24 GHz to 157 GHz Using Remotely Sensed Aircraft Data, *Remote Sens.*
483 *Environ.*, 73, 323-336, [https://doi.org/10.1016/S0034-4257\(00\)00108-5](https://doi.org/10.1016/S0034-4257(00)00108-5), 2000.



- 484 Morland, J. C., Metcalfe J., and Walker A.: Microwave remote sensing of soil moisture in
485 southern Ontario: Aircraft and satellite measurements at 19 and 37 GHz, *Radio Sci.*, 38, 8073,
486 doi:10.1029/2002RS002677, 2003.
- 487 Njoku, E.G., and O'Neill P. E.: Multifrequency microwave radiometer measurements of soil
488 moisture, *IEEE Trans. Geosc. Remote Sens.*, 20, 468-475, doi:10.1109/TGRS.1982.350412,
489 1982.
- 490 Ruston R. C., Vonder Haar T. H.: Characterization of summertime microwave emissivity from the
491 Special Sensor Microwave Imager over the conterminous United States, *J. Geophys. Res.*, 109,
492 D19103, doi:10.1029/2004JD004890, 2004.
- 493 Prigent, C., W. B. Rossow, E. Matthews, Microwave land surface emissivities estimated from
494 SSM/I observations, *J. Geophys. Res.*, 102, 21867-21890,
495 <https://doi.org/10.1029/97JD01360>, 1997.
- 496 Prigent, C., Rossow, W. B., Matthews, E., and Marticorena, B.: Microwave radiometric signatures
497 of different surface types in deserts, *Journal of Geophysical Research*, 104, 12147-12158, doi:
498 10.1029/1999JD900153, doi:10.1029/1999JD900153, 1999.
- 499 Prigent, C., Wigneron, J. P., Rossow, W. B., and Pardo-Carrionet, J.R.: Frequency and angular
500 variations of land surface microwave emissivities: Can we estimate SSM/T and AMSU
501 emissivities from SSM/I emissivities? *IEEE Trans. Geosci. Remote sensing*, 38, 2373-2386,
502 doi:10.1109/36.868893, 2000.
- 503 Prigent, C., Aires F., and Rossow W. B.: Land surface microwave emissivities over the globe for a
504 decade, *Bull. Amer. Meteorol. Soc.*, **87**, 1573 - 1584,
505 <https://doi.org/10.1175/BAMS-87-11-1573>, 2006.
- 506 Schwartz, C. S., Liu, Z. Q., Chen, Y., Huang, X.Y.: Impact of assimilating microwave radiances
507 with a limited-area ensemble data assimilation system on forecasts of Typhoon Morakot,
508 *Weather Forecasting*, 27, 424-437, <https://doi.org/10.1175/WAF-D-11-00033.1>, 2012.
- 509 Ulaby, F. T., Moore, R. K., Fung, A. K.: *Microwave Remote Sensing: Active and Passive. Vol. 3:*
510 *From Theory Applications.* Addison-Wesley Publ. Company, Readings, Massachusetts, 1986.
- 511 Wang, J. R. and Choudhury, B. J.: Remote sensing of soil moisture content over bare field at 1.4
512 GHz frequency, *J. Geophys. Res.*, 86, 5277-5282, 1981.
- 513 Wigneron, J. P., Guyon, D., Calvet, J. C., Courrier G., Bruguier N.: Monitoring coniferous forest
514 characteristics using a multifrequency microwave radiometry, *Remote Sens. Environ.*, 60,
515 299-310, doi:10.1016/S0034-4257(96)00212-X, 1997.
- 516 Weng, F., Yan, B., Grody N.C.: A microwave land emissivity model, *J. Geophys. Res.*, 106,
517 20,115-20,123, <https://doi.org/10.1029/2001JD900019>, 2001.
- 518 Xie, Y., Shi, J., Ji, D., Zhong, J., Fan, S.: A Parameterized Microwave Emissivity Model for Bare
519 Soil Surfaces, *Remote sensing*, 9, 155-170, <https://doi.org/10.3390/rs9020155>, 2017.